Development of sodium-ion conducting biopolymer electrolyte membrane based on Agar-Agar with sodium perchlorate ($NaClO_4$) using ethylene carbonate (EC) as a plasticizer for primary Na-ion battery

S. Sowmiya[a,*], C. Shanthi[a], S. Selvasekarapandian[b,c]
[a]*Department of Physics, Sona College of Technology, Salem 636005, Tamil Nadu, India*
[b]*Material Research Centre, Coimbatore 641045, Tamil Nadu, India*
[c]*Department of Physics, Bharathiar University, Coimbatore 641046, Tamil Nadu, India*

The current study investigates the sodium ion conductivity of ethylene carbonate (EC) integrated biopolymer membranes made of agar-agar and sodium perchlorate in various concentrations. The facile solution cast approach is employed to fabricate the biopolymer membranes. The prepared biopolymer membranes are characterized by XRD, FTIR, DSC, AC Impedance, TGA, CV, and LSV techniques. X-ray diffraction analysis (XRD) studies the degree of crystalline/amorphous nature of the membranes. Fourier transform infrared spectroscopy (FTIR) confirms the complexation between salt and polymer. Adding sodium salt and incorporating a plasticizer improves the ionic conductivity of pure agar-agar from 3.12×10^{-7} S cm^{-1} to 3.15×10^{-3} S cm^{-1}. Differential scanning calorimetry (DSC) studies the glass transition temperature (T_g) trend with salt concentration. The highest conducting biopolymer membrane exhibits a very low T_g value of 22.05°C. Thermogravimetric analysis (TGA) examines the thermal stability of the membranes. Wagner's DC polarization technique evaluates the transference number for the prepared membrane. The electrochemical and cycling stability of the highest conducting membrane was studied by linear sweep voltammetry (LSV) and cyclic voltammetry (CV), respectively. The findings promote the development of a primary sodium ion conducting battery with the highest-performing biopolymer membrane. The battery's performance has been studied with two different cathode materials (V_2O_5 and MnO_2) and the highest remarkable open circuit voltage (OCV) of 3.13 V was achieved when V_2O_5 was used as a cathode.

(Received September 13, 2023; Accepted December 11, 2023)

Keywords: Biopolymer membrane, Plasticizer, Deconvolution, Conductivity studies, Cyclic voltammetry

1. Introduction

Research is being done to create biobased polymers to solve environmental challenges as part of a contemporary global objective to make an environmentally friendly process for a biobased future [1]. The increase in polymer research, particularly about biopolymers, is envisaged to satisfy future industrial demands [2]. The primary benefits of polymer electrolytes (PE) are their mechanical qualities, more accessible fabrication into thin films, and electrochemical devices; they can form good contact with electrode material [3]. Because of their usage in solid-state electrochemical devices, ion-conducting PE has garnered attention in solid-state ionics. [4]. The main fundamental goal of polymer research is synthesizing polymeric systems with excellent ionic conductivity. Due to their strong ionic conductivity, broad electrochemical stability, and high energy density, they can be electrolytes in solid-state batteries [5]. Solid polymer electrolytes (SPE) can develop a wide range of solid-state electrochemical devices like batteries, fuel cells, sensors, and solar cells [6,7]. Biopolymers and their based products have been studied for a diverse range of novel applications in which they can provide a substitute for the usage of existing

* Corresponding author: sowmiconfi@gmail.com
https://doi.org/10.15251/DJNB.2023.184.1537

polymer-composite materials and non-degradable synthetic polymers [8]. Biopolymers, an affordable and renewable resource, can be employed as sustainable organic electrodes for sodium-ion batteries with extremely effective electrochemical energy storage [9].

Several works published recently focused on the addition of plasticizers to biopolymer membranes. Plasticizers are non-volatile substances when introduced to a polymer, improving their processability and flexibility [10]. With the incorporation of the plasticizer molecules, ionic conductivity enhanced as a result decrease in T_g and crystalline regions [11,12]. Ethylene and propylene carbonates (EC and PC) have been widely used to plasticize polymeric membranes because of their relative permittivity [13,14]. Compared to PC, EC has generally shown a better effect in enhancing ionic conductivity [14]. In the impact of EC plasticizer on agar-agar: NH_4Br-based solid polymer electrolytes, 0.3% EC added to 50% agar/50% NH_4Br enhances the ionic conductivity of 3.73×10^{-4}, which was reported [15]. With the introduction of the plasticizer (EC), the ionic conductivity of PE $(PEO)_9 LiCF_3SO_3$ is enhanced from 1.8×10^{-4} to 2.7×10^{-2} m S cm^{-1} has been reported [16]. A filler-filled PEO-based electrolyte increases the ion conductivity up to 0.15 mS cm^{-1} by adding a 50wt% of EC [17].

Agar is a polysaccharide derived from certain red seaweeds [18]. Agar, like various gelling gums, is primarily utilized as a gelling and thickening agent in various applications in industries including biotechnology, food, pharmaceuticals, and biomedicine [19]. It is an ideal replacement resource for films that decompose as it has good mechanical strength with water resistance [20]. Agar has been able to form films successfully examined by various researchers [21-27]. Agar-agar with LiCl exhibits the highest ionic conductivity of $3.12 \pm 0.11 \times 10^{-2}$ S/cm reported for Li-ion conducting battery performance [28]. The effects of glycerol (GLY) addition on the morphological and physicochemical characteristics of PVA-agar films were described [29]. There are several methods to extract agar, but the syneresis method has shown the most promising outcomes because of its precision and cost-effectiveness [30]. Agar was used to prepare the optimal gel electrolyte for Mg-air batteries and reported an ionic conductivity of 8.62×10^{-2} S cm^{-1} [31]. Agar-based membranes can also be synthesized for microbial fuel cells, and their proton conductivity was found to be 1.81-2.43 mS cm^{-1} [32]. Agar and polyacrylamide (PAM) were combined to create an agar-based composite hydrogel PE for Zn-ion battery performance [33].

The sodium-based solid electrolyte's mechanical properties, chemical stability, and ionic conductivity were studied. They exhibited better cost efficiency and were the recommended choice for economic energy storage [34]. The pioneering study by Wright et al. in 1973 gave rise to PE, which was extensively studied in lithium batteries. Still, recent research articles on Na-ion-conducting PE demonstrate that they have turned their attention to sodium batteries [35]. Thus, sodium has been proposed as a possible replacement for lithium and is seen as a viable alternative to energy storage devices. Studies on the electrical properties of SPE have garnered a lot of attention in rechargeable metal-ion battery applications. Electrochemical energy storage, particularly batteries, can potentially enhance pollution reduction and the use of finite resources effectively [36]. Polymer electrode materials have been proven to offer great potential for application in Na-ion batteries because of the abundance of sodium [37]. Research on Na ion batteries is rapidly reducing the cost of using a large amount of energy storage from renewable resources [9]. PEO-based PE complexed with sodium salts $NaFeF_4$ for applying sodium-ion battery was studied [38]. GO-doped PEO/PVP complexed with $NaIO_4$ salt was prepared, and the maximum conductivity of 1.57×10^{-7} S/cm was reported [39]. The primary sodium-ion battery was constructed with salt $NaClO_4$ and tamarind seed, exhibiting the ionic conductivity of 1.70×10^{-3} S cm^{-1}[40].

In the present study, the solution casting approach prepares the biopolymer membrane pure agar-agar and sodium perchlorate ($NaClO_4$) with various concentrations. The prepared solid biopolymer electrolyte (BPE) membrane is studied and characterized using XRD, FTIR, DSC, TGA, CV, LSV, and AC Impedance spectroscopy techniques. Finally, the primary sodium-ion battery was fabricated using the highest ionic conducting PE membrane, sodium metal as an anode, and V_2O_5 and MnO_2 as two different cathode materials; Open circuit voltage and current are measured.

2. Experimental method

The solid BPE membrane pure agar-agar with several compositions of agar-agar with $NaClO_4$ has been prepared using the solution casting technique. The different weight percentage of agar-agar: $NaClO_4$ membrane and agar-agar: $NaClO_4$ membrane with EC was calculated as 60%agar :40% $NaClO_4$, 50%agar :50% $NaClO_4$, 40%agar :60% $NaClO_4$, 30%agar :70% $NaClO_4$, 40%agar :60% $NaClO_4$ with 0.5 wt.% of EC, and, 40%agar :60% $NaClO_4$ with 0.7wt.% of EC. The calculated weight percentage of agar-agar was added slowly into the hot water and kept under stirring at a temperature of 85°C. Then, $NaClO_4$ at different weight percentages of (40%, 50%, 60%, 70%, 60% with 0.5 wt.% of EC, and 60% with 0.7 wt.% of EC) was added slowly to the transparent agar-agar solution. The mixture is continuously stirred for two hours then the solution becomes homogenized. The obtained homogenized solution was then cast in the polypropylene petri dish placed in a vacuum oven, and dried at 60°C. After 24 hours, the transparent films are obtained. The graphical abstract of the preparation method is shown in Scheme 1. The sample code is represented in Table 1.

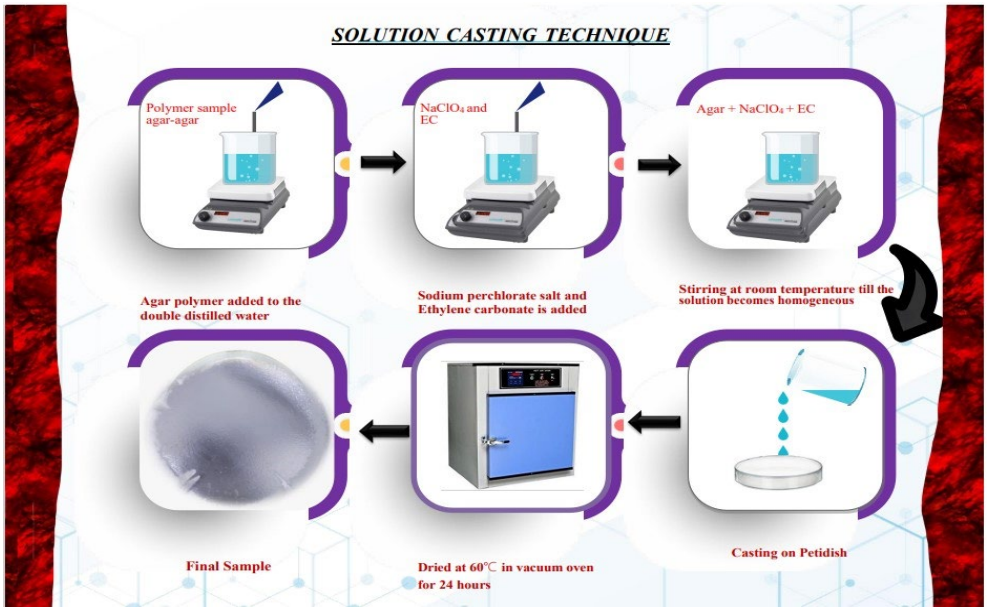

Scheme 1. Graphical Abstract.

Table 1. Sample code of pure agar-agar, sodium perchlorate, ethylene carbonate, and compositions of agar-agar: $NaClO_4$ at different molecular ratios.

Sample and its Molecular ratios	Sample Code
Pure agar-agar	AA
Sodium perchlorate	SCL
Ethylene Carbonate	EC
60%agar :40% $NaClO_4$	AASCL1
50%agar :50% $NaClO_4$	AASCL2
40%agar :60% Na ClO_4	AASCL3
30%agar:70%$NaClO_4$	AASCL4
40%agar :60% $NaClO_4$ with 0.5 wt.% of EC	AASCL3 EC1
40%agar :60% $NaClO_4$ with 0.7 wt.% of EC	AASCL3 EC2

2.1. Characterization Techniques

XRD patterns for produced samples were recorded using BRUKER ECO D8 ADVANCE equipment with Cu-K radiation at (2θ) 0°-90° range to determine whether the electrolytes are amorphous or crystalline. To investigate the complexation behavior of salt and polymer, the FTIR spectra for the films were collected at room temperature using a spectrometer with a resolution of $1cm^{-1}$ called the SHIMADZU-IR Affinity-1. The produced sample was examined using DSC measurement (Q 20 V24.10 Build 122) TA equipment under a nitrogen atmosphere at a heating rate of 10°C min-1. The thermal stability of the polymer membrane was analyzed using the DSC-TGA standard (SDT Q600 V20.9 Build 20). The samples are heated from 50-700°C at the heating range of 10°C/min and a sample weight of around 2.5 mg. The resistivity of the electrolyte is determined using AC Impedance tests in the frequency range of 42-1 MHz by HIOKI 3532 LCR Tester. The transference number of the polymer sample was assessed using Wagner's DC polarization method. The prepared membrane was positioned between stainless steel electrodes and connected in series to a 1.0 V DC power supply. Thus observed the initial and final currents as a function of time. The cycling stability of the high-conducting polymer membrane was examined by the Electrochemical Analyzer CHI600C Series at a scan rate of 0.1 V/s in the potential range of -1 to +1. The electrochemical stability of the polymer membrane was evaluated using a multichannel workstation, the Bio-Logic VSP-300 (France), at a scan rate of 1 mV/sec.

2.2. Anode and Cathode Preparation

Anode: Sodium (Na) metal (1mm thickness, 12mm diameter) is used as an anode material.

Cathode: In this study, two different cathode materials (V_2O_5 and MnO_2) are used. The cathode material (V_2O_5), graphite, and PE are mixed well. The well-combined mixture was ground for an hour and kept for drying. Then the necessary quantity of the sample was pelletized using a pelletizer at the thickness of 12mm. Similarly, the mixture of MnO_2, graphite, and PE was also prepared and pelletized. Thus, the two different cathode materials (pellets) are ready to fabricate two primary batteries.

2.3. Primary battery fabrication

The optimum conducting BPE membrane is placed between the anode (Na metal) and Cathode (V_2O_5 and MnO_2). The cell with sodium metal, BPE membrane, and V_2O_5 is assembled in the battery holder. Similarly, another cell with sodium metal, BPE membrane, and MnO_2 is placed in the battery holder. Thus, the two different constructed cells are fabricated. Then the assembled battery's open circuit voltage (OCV) is measured, and the performance is studied using a load of 100k.

3. Results and discussion

3.1. X-ray diffraction method (XRD)

The amorphous/crystalline nature of the prepared BPE membrane has been analyzed by X-ray diffraction method. Fig.1 represents the XRD pattern for AA, AASCL1, AASCL2, AASCL3, AASCL4, AASCL3 EC1, and AASCL3 EC2. For AA, the peak was observed at 2θ = 13°, 20° and 30°. The peak values obtained for AA were reported earlier [41]. The peak at 2θ = 20° in AA gets broader in the salt-doped samples due to the addition of the SCL salt, whereas the peak value at 30° for AA has been reduced in AASCL1, and it disappeared in other compositions of AASCL2, AASCL3, AASCL4, AASCL3 EC1, and AASCL3 EC2. Thus, adding the salt perturbed the polymer network, and the polymer became more amorphous. The amorphous nature is more for the polymer membrane AASCL3 than AA, AASCL1, and AASCL2. This shows that the degree of crystallinity decreases when SCL salt is added, and the amorphicity of the complex membrane increases simultaneously [42]. The reduced intensity of the peak and increased broadness follow Hodge et al.'s criterion [43]. Further, with the addition of 70% SCL salt in 30% AA, it is observed that there is a decline in amorphous nature. This is due to the aggregation of the salt. Adding a plasticizer EC (0.5 wt.% of EC and 0.7 wt.% of EC) to the composition AASCL3 improves the amorphous content. It is observed that the composition AASCL3 EC1 has a more amorphous

nature than any other membrane. Using a plasticizer aggregation of ions could be dispersed. Thus, the enhanced ionic diffusivity caused by this amorphous nature leads to stronger ionic conductivity [44]. Fig. 1(a) shows a deconvoluted pattern for AA, AASCL1, AASCL2, AASCL3, AASCL4, AASCL3 EC1, and AASCL3 EC2.

The crystalline percentage for AA, AASCL1, AASCL2, AASCL3, AASCL4, AASCL3 EC1, and AASCL3 EC2 is calculated in Table 2 using the formula,

Crystalline percentage formula = (crystalline area / total area) ×100

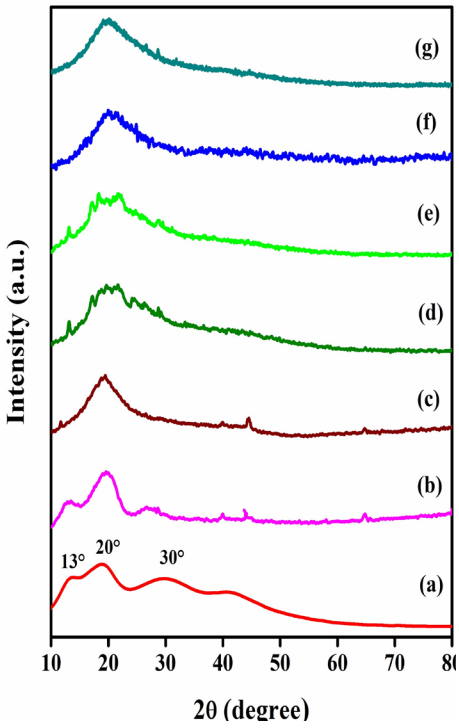

Fig. 1. XRD patterns of (a) AA, (b) AASCL1, (c) AASCL2, (d) AASCL3, (e) AASCL4, (f) AASCL3 EC1 and (g) AASCL3 EC2.

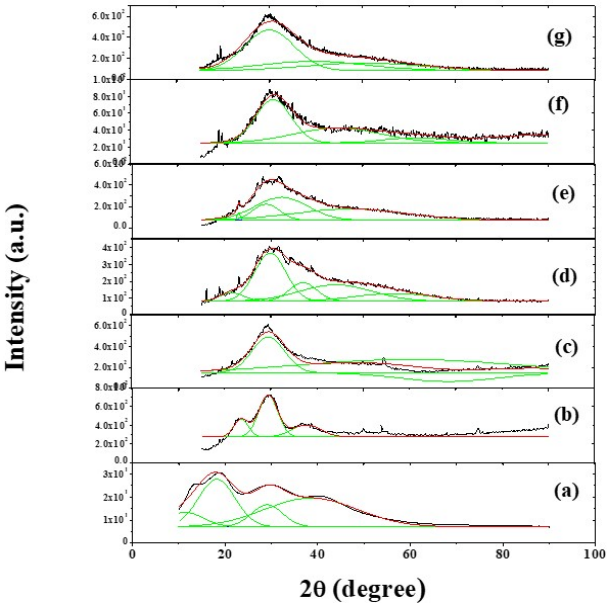

Fig. 2. (a) Deconvoluted XRD patterns of (a) AA, (b) AASCL1, (c) AASCL2, (d) AASCL3, (e) AASCL4, (f) AASCL3 EC1 and (g) AASCL3 EC2.

Table 2. Crystallne Percentage.

S. No	Sample	Crystalline Percentage (%)
1	AA	30.83
2	AASCL1	27.05
3	AASCL2	24.83
4	AASCL3	23.02
5	AASCL4	25.92
6	AASCL3 EC1	18.60
7	AASCL3 EC2	20.42

3.2. Fourier transform infrared spectroscopy (FTIR)

The FTIR spectra for AA and different concentrations of AA: SCL in the wavenumber range from 4000-680 cm^{-1} are shown in Fig 2. The FTIR peaks and their assignments are tabulated in Table 3. The observed FTIR spectra for AA agreed with the prior report [15]. The broadband in AA at 3323cm^{-1} is attributed to OH stretching. This peak is due to the several OH groups present in AA. This OH peak shifts to 3428cm^{-1}, 3415 cm^{-1}, 3433cm^{-1}, 3429 cm^{-1}, 3423 cm^{-1}, and 3427 cm^{-1} for different concentrations of AA and SCL. Thus, the peak shifting is because of the interaction of the polymer AA with SCL salt. The band at 2921cm^{-1} in AA is attributed to CH_2 stretching and it has been shifted to 2922 cm^{-1}, 2926 cm^{-1}, 2923 cm^{-1}, 2931 cm^{-1}, 2929 cm^{-1}, and 2917 cm^{-1} for AASCL1, AASCL2, AASCL3, AASCL4, AASCL3 EC1, and AASCL3 EC2 respectively. This verifies the complex formation between the salt and the host polymer. The band at 1771 cm^{-1}, and 1770 cm^{-1} in AASCL3 EC1 and AASCL3 EC2 corresponds to C=O stretching. In the plasticized polymer-salt complex, this C=O bond appears to be broadened, indicating that the plasticizer interacts with the polymer [15].

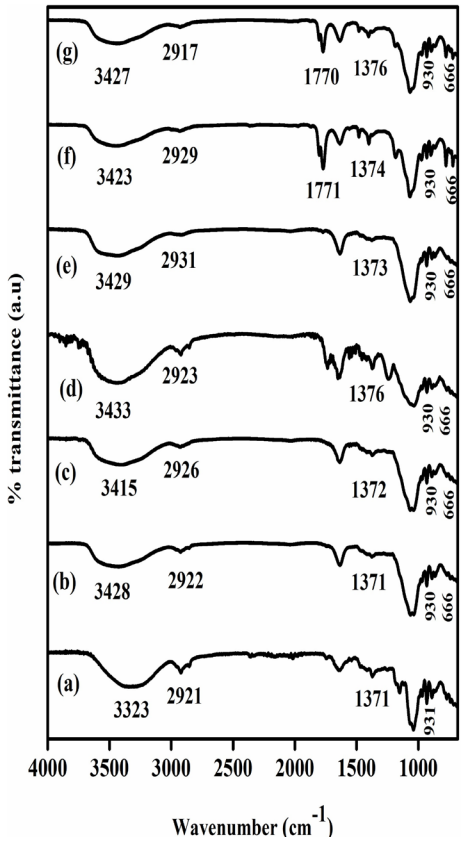

Fig. 3. FTIR spectra of (a) AA, (b) AASCL1, (c) AASCL2, (d) AASCL3, (e) AASCL4, (f) AASCL3 EC1 and (g) AASCL3 EC2.

The broad peak's intensity at 1641cm^{-1} for AA corresponding to C=O stretching decreases with increased salt concentration. The absorption peak at 1371cm^{-1} for AA belongs to CH_2 bending which is shifted to 1371cm^{-1}, 1372cm^{-1}, 1376cm^{-1}, 1373 cm^{-1},1374cm^{-1}, and 1376cm^{-1} for AASCL1, AASCL2, AASCL3, AASCL4, AASCL3 EC1, and AASCL3 EC2 respectively. This shift in the position of the peak shows the complex formation between AA and SCL salt. The peak at 931cm^{-1} in polymer membrane AA is attributed to 3,6-anhydrogalactose bridges [45]. Two vibrational peaks are observed at 930cm^{-1} and 666cm^{-1} in the salt-doped samples. The band at 930cm^{-1} has been assigned to the symmetric stretching vibration (ClO_4^-), [46] which overlaps with the pure sample, and the band at 666cm^{-1} has been assigned to asymmetric bending vibration (ClO_4^-) [47] for the salt-doped samples. Thus, the changes in the intensity and frequency, the interaction of salt with the polymer, and a slight shift in the position of peaks confirm the complex formation between the polymer AA and SCL salt.

Table 3. Absorption peaks for AA and various ratios of AA with SCL polymer electrolytes and their Assignment.

Wavenumber(cm^{-1})							Assignment
AA	AASCL1	AASCL2	AASCL3	AASCL4	AASCL3 EC1	AASCL3 EC2	
3323	3428	3415	3433	3429	3423	3427	O-H stretching
2921	2922	2926	2923	2931	2929	2917	CH_2 stretching
-	-	-	-	-	1771	1770	C=O stretching
1641	1636	1634	1634	1635	1633	1634	C=O stretching
1371	1371	1372	1376	1373	1374	1376	CH_2 bending
1066	1066	1064	1063	1065	1065	1065	C-O-C Stretching
931	930	930	930	930	930	930	3,6-anhydrogalactose bridges and symmetric stretching vibration (ClO_4^-)
-	666	666	666	666	666	666	Asymmetric bending vibration (ClO_4^-)

The frequency change in FTIR vibration can be explained using force constant calculation. The force constant for O-H stretching for all the samples is calculated, and the values are listed in Table 4.

Table 4. Force Constant values of the prepared membranes for O-H stretching.

Sample	OH Stretching Wavenumber(cm^{-1})	Force Constant N/cm
AA	3323	612.50
AASCL1	3428	651.86
AASCL2	3415	647.02
AASCL3	3433	652.69
AASCL4	3429	652.26
AASCL3 EC1	3423	650.04
AASCL3 EC2	3427	650.21

Using Hooke's relation, the force constant k is determined [28]

$$\bar{\upsilon} = \frac{1}{2\pi c}\sqrt{k/\mu}\ \text{N/cm}$$

where $\bar{\upsilon}$ is Wavenumber (cm^{-1})

c – Velocity of light (3×10^{10} cms^{-1})
k – Force constant (Newton/cm)
μ – Reduced mass.
The reduced mass (μ) is given by

$$\mu = \frac{m_1 \times m_2}{m_1 + m_2}$$

From Table 4, the force constant value for AA is 612.50 N/cm. As the concentration of the salt increases, enhances the force constant, where the bond length reduces. A decline in bond length results in increasing vibrational frequency. This confirms the formation of the complex between the salt and the polymer. Scheme 2 shows the interaction between the polymer AA and the salt SCL.

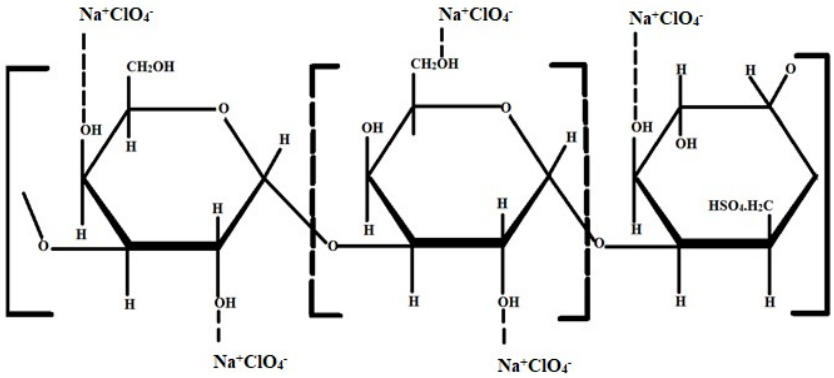

Scheme 2. Possible interaction between the polymer matrix AA and SCL

3.3. Differential Scanning Calorimetry (DSC)

DSC spectra of the prepared biopolymer membrane AA, AASCL1, AASCL2, AASCL3, AASCL4, AASCL3 EC1, and AASCL3 EC2 are shown in Fig. 3 and the results are tabulated in Table 5. A single Tg value of 69°C shown in Fig.3 (a) for the AA sample agrees with the prior report [41].

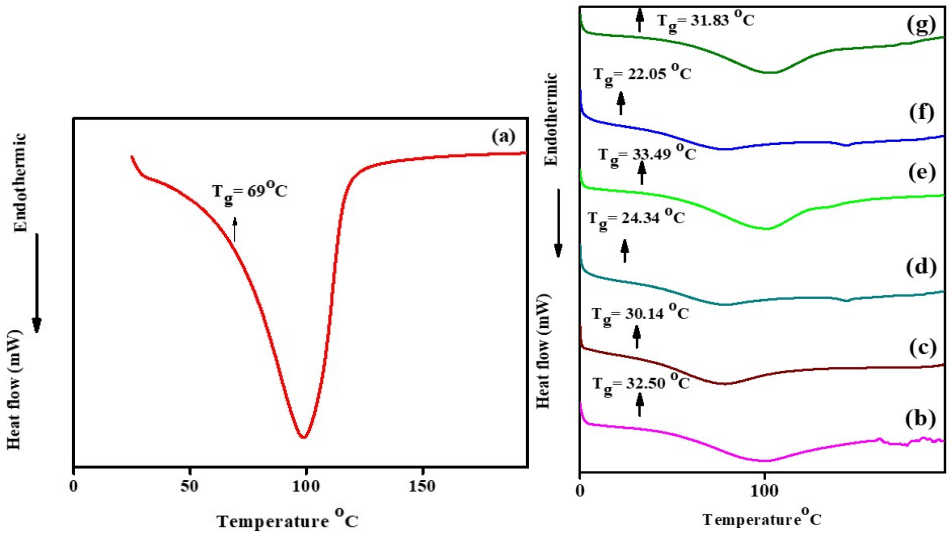

Fig. 3. DSC analysis of the polymer membrane (a) AA, (b) AASCL1, (c) AASCL2, (d) AASCL3, (e) AASCL4, (f) AASCL3 EC1 and (g) AASCL3 EC2.

Table 5. Glass transition temperature (T_g) for different compositions of the polymer membrane.

Compositions of polymer membrane	(T_g) value °C
AA	69
AASCL1	32.50
AASCL2	30.14
AASCL3	24.34
AASCL4	33.49
AASCL3 EC1	22.05
AASCL3 EC2	31.83

Including salt SCL reduces the T_g for AASCL1, AASCL2, AASCL3, AASCL4, AASCL3 EC1, and AASCL3 EC2 shown in Fig. 3. (b, c, d, e, f, g). This decline value in T_g suggests that the polymer backbone's softening contributes to increased segmental motion [48]. AASCL3, one of the salt-doped samples, exhibited a low T_g value of 24.34°C, leading to the polymer chain's rapid segmental mobility [49]. The T_g value of AASCL4 has been enhanced by the addition of 70% of SCL salt. This might be due to the excess SCL salt, which lowers the polymer chain flexibility [50]. Since the rise of the T_g value in AASCL4, the plasticizer was added to the polymer membrane AASCL3 as it exhibited a low T_g. In this study, adding 0.5 wt.% of the plasticizer EC to the sample AASCL3, the T_g value decreases from 24.34°C to 22.05°C. Adding a plasticizer lowers the T_g value and raises the segmental motion of the polymer chain, which was reported earlier [51]. Thus, the membrane AASCL3 EC1 exhibited a lower T_g value than any other composition.

3.4. AC Impedance Spectroscopic Analysis

The ionic conductivity of the BPE membrane is determined by the AC Impedance spectroscopic analysis that reigns the battery's overall performance. Fig. 4 depicts the cole-cole plot of the membrane AA and the various concentrations of AA with salt SCL.

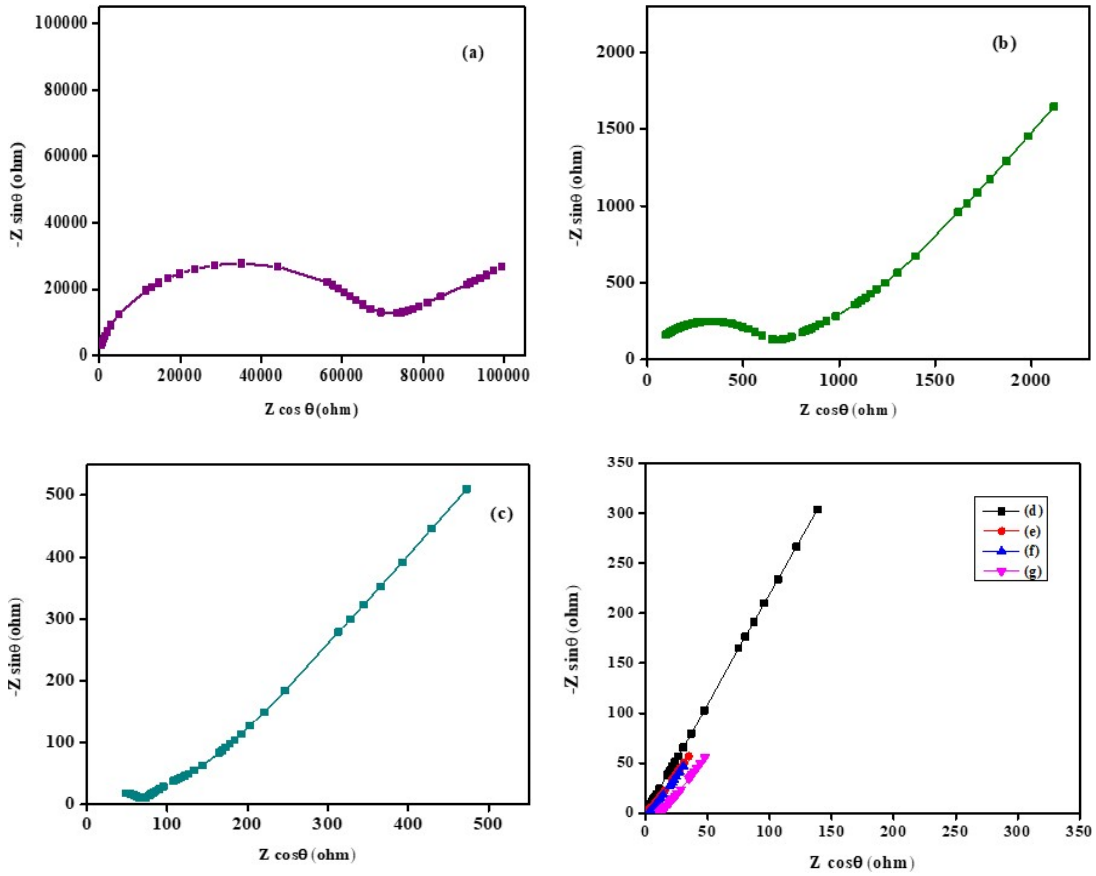

Fig. 4. The cole-cole plot of (a) AA, (b) AASCL1, (c) AASCL2, (d) AASCL3, (e) AASCL4, (f) AASCL3 EC1 and (g) AASCL3 EC2.

The high-frequency semicircle for the membrane AA in Fig. 4 (a) is due to the bulk effect of the PE. The semicircle disappears with the addition of the salt SCL, and a low-frequency spike region is observed because of the double-layer capacitor at the electrode-electrolyte interface [52] shown in Fig. 4 (b, c, d, e, f, g).

The equivalent circuits for AA are the parallel combination of a bulk capacitor and bulk resistance shown in Fig. 5(a). The equivalent circuits for AASCL1, AASCL2, AASCL3, AASCL4, AASCL3 EC1, and AASCL3 EC2 are shown in Fig. 5(b).

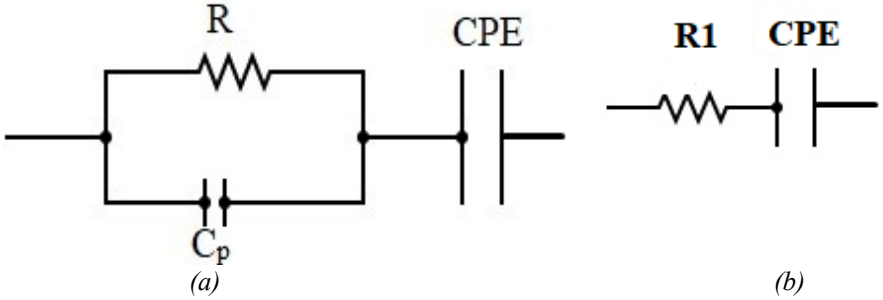

Fig. 5. Equivalent circuit for the membrane (a) AA, (b) AASCL1, AASCL2, AASCL3, AASCL4, AASCL3 EC1, AASCL3 EC2.

The ionic conductivity equation is used to depict the conductivity value for the polymer electrolyte membrane [53].

$$\sigma = l/AR_b \, S \, cm^{-1}$$

Using the prepared BPE membrane, the Thickness (l) and area (A) have been observed. By using the Boukamp software [54], Bulk resistance (R_b) and electrochemical impedance spectroscopy (EIS) are obtained. The ionic conductivity for AA is 3.12×10^{-7} Scm^{-1}. The conductivity of the BPE membrane has increased up to AASCL3, as a salt concentration increases. When 70% of SCL salt is added to AASCL4, the ionic conductivity reduces to 3.73×10^{-4} Scm^{-1}. The diminution in ionic conductivity value might be attributed to the formation of ion aggregates. Using a plasticizer aggregate of ions could be dispersed. The present study uses ethylene carbonate (EC) as a plasticizer. By adding a plasticizer 0.5 wt.% of EC to AASCL3, the ionic conductivity has increased to the order of 3.15×10^{-3} Scm^{-1}. When the plasticizer (EC) concentration is raised to 0.7 wt.% to AASCL3, the ionic conductivity is determined to be 1.62×10^{-3} Scm^{-1}. Comparatively, the AASCL3 EC1 membrane is found to have the highest ionic conductivity. Thus the primary function of a plasticizer in a host polymer is to reduce the electrolyte's viscosity and help in salt dissociation, increasing the number of charge carriers [55]. AASCL3 EC1 has a maximum ionic conductivity since it has a high charge carrier concentration, a high amorphous nature (confirmed by XRD), and a low T_g value (confirmed by DSC). Agar-agar with LiCl shows the highest ionic conductivity of $3.12 \pm 0.11 \times 10^{-2}$ S/cm for the reported Li-ion conducting battery performance [28]. The impedance of the (CPE) constant phase element is given by [49]

$$Z_{CPE} = 1/Q_0(j\omega)_n$$

n and Q_0 are frequency-independent factors. The value of n=0 and n=1 represents pure resistor and pure capacitor, respectively. The value of CPE, n, ionic conductivity for the pure polymer membrane, and the different concentrations of salt with polymer are shown in Table 6. The CPE value for AA is 1.3846×10^{-1} μF. The value of n for AA is 0.9272.

Table 6. Conductivity parameters of polymer membrane AA and AA: SCL with different concentrations.

Compositions of polymer membrane	CPE (μF)	n (no unit)	Ionic conductivity (σ, Scm^{-1})
AA	1.3846×10^{-1}	0.9272	3.12×10^{-7}
AASCL1	3.7506×10^{-5}	0.2367	4.4×10^{-6}
AASCL2	2.6996×10^{-5}	0.5008	5.02×10^{-5}
AASCL3	4.3485×10^{-4}	0.7284	7.37×10^{-4}
AASCL4	2.6683×10^{-5}	0.4832	3.73×10^{-4}
AASCL3 EC1	3.2516×10^{-4}	0.6541	3.15×10^{-3}
AASCL3 EC2	3.5616×10^{-4}	0.6174	1.62×10^{-3}

3.5. Conductance spectra

The conductance spectra of all the prepared BPE membranes AA, AASCL1, AASCL2, AASCL3, AASCL4, AASCL3 EC1, and AASCL3 EC2 are shown in Fig. 6. Conductance spectra typically consist of three distinct regions: low-, mid-, and high-frequency region. Space charge polarization, and DC conductivity of all the prepared BPE membranes due to the ion migration to the neighboring sites are observed in the low- and mid-frequency regions respectively, and bulk relaxation phenomena are observed in the high-frequency regions [49]. In this work, the BPE membrane AA conduction spectra comprise low-, mid-, and high-frequency regions. Whereas other membranes exhibit low- and mid-frequency regions. The mid-frequency-independent plateau area is extrapolated to zero frequency (log σ-axis) to determine the DC ionic conductivity [56]. Thus, the DC conductivity value determined by conduction spectra and the Cole-Cole plot accord well with one another.

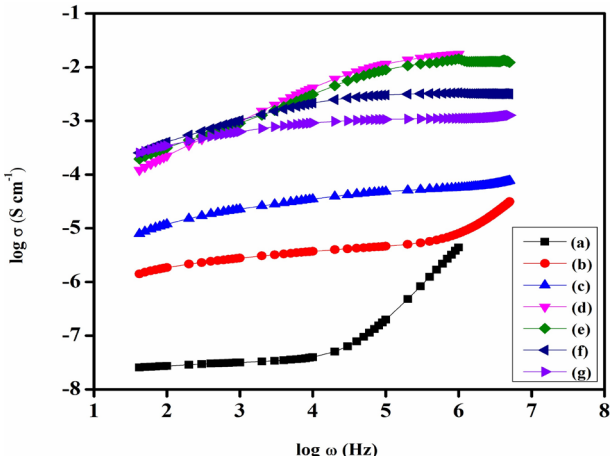

Fig. 6. Conductance spectra of the polymer membrane (a) AA, (b) AASCL1, (c) AASCL2, (d) AASCL3, (e) AASCL4, (f) AASCL3 EC1 and (g) AASCL3 EC2.

3.6. Thermogravimetric analysis

The thermal stability of the prepared BPE membrane has been examined by thermogravimetric analysis. The TGA curves of AA and the high ionic conductivity of the plasticized sample AASCL3 EC1 are shown in Fig. 7. The different stages of degradation and weight loss percentages for AA and AASCL3 EC1 are observed in the figure. From the figure, it has been analyzed that the first stage of degradation starts from 50℃ and continues to 249℃ with a weight loss of 17.1% for AA and at 50℃ to 175℃ occurs for AASCL3 EC1 with a weight loss of 15.9%. Thus, the reduction of moisture content in the membrane causes the first stage of degradation and weight loss [57]. Then the second stage of degradation occurs at 249-346℃ with a weight loss of 45.3% for AA due to the destruction of agarose and agro pectin [58]. Similarly, for AASCL3 EC1, the degradation starts at 175℃ and ends at 240℃ in the second stage with a weight loss of 51.2% due to the destruction of the polymer-salt matrix [59]. The third stage of degradation starts from 346-687℃ with a weight loss of 45.3% for AA, and the complete degradation occurs at 687℃ with a weight loss of 7.5% for AASCL3 EC1. This is due to carbonization and ash formation. [59].

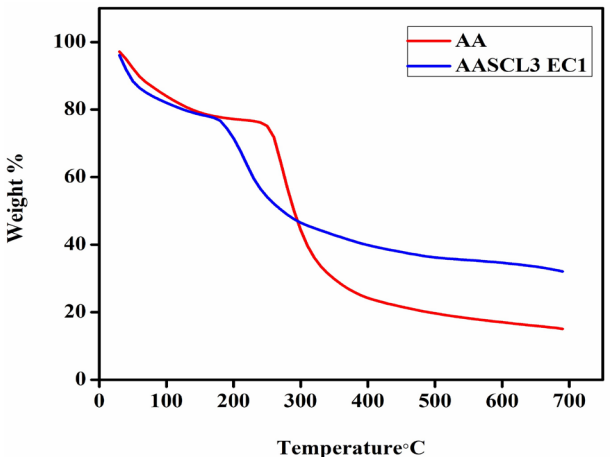

Fig. 7. Thermal stability of the polymer membrane AA and AASCL3 EC1.

3.7. Transference number measurement

3.7.1. Wagner's Polarization Method

Using DC Wagner's polarization method, the ionic transference number of the highest conducting membrane AASCL3 EC1 is determined by applying 1.0 V across the cell. Fig 8 shows the Time vs. polarization current plot for the plasticized membrane AASCL3 EC1. From Figure 8, the maximum current has appeared with time, then it gets depleted and reaches a steady state [60]. The total ionic transference number for the highest conducting membrane AASCL3 EC1 is observed to be 0.92. It is calculated by using the formula [61,62],

$$(t_{ion}) = I_i - I_f / I_i$$

$$(t_{ele}) = I_f / I_i$$

I_i -initial current and I_f - final current.

Thus, the conductivity in the electrolyte membrane is due to ions.

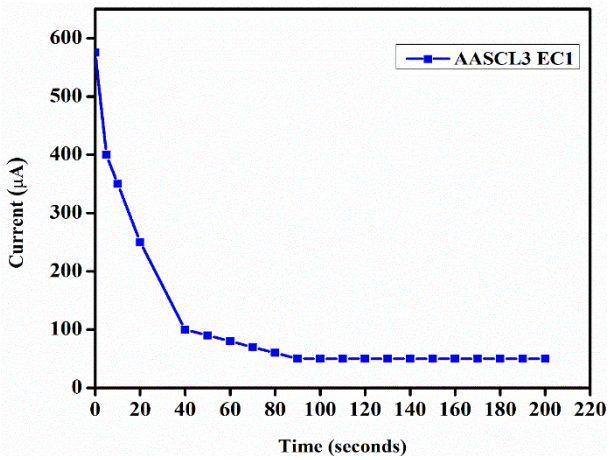

Fig. 8. Plot of Polarization current versus time for the polymer membrane AASCL3 EC1.

3.8. Linear sweep voltammetry (LSV)

The electrochemical stability window has been measured using linear sweep voltammetry for AASCL3 and AASCL3 EC1 samples. With a scan rate of 1 mVs^{-1}, the voltage is between 0 and 5 V. Fig. 9 (a) and (b) depict the fluctuation of current with respect to voltage. The electrochemical stability window value for AASCL3 and AASCL3 EC1 samples is found to be 2.82 and 3.16 V respectively. The electrochemical window of the sample enhanced from 2.82 to 3.16 V due to its plasticizing effect [63]. The voltammogram shows that the current remains unchanged up to 3.16 V for the highest conducting BPE membrane AASCL3 EC1. This clearly shows that the electrolyte membrane is stable. Thus, the electrochemical stability of the prepared polymer membrane is suited for electrochemical devices. In the present study, the value of the electrochemical stability window is higher than that reported by Selvalakshmi et al. with a value of 2.5 V for agar-NH_4Br [51].

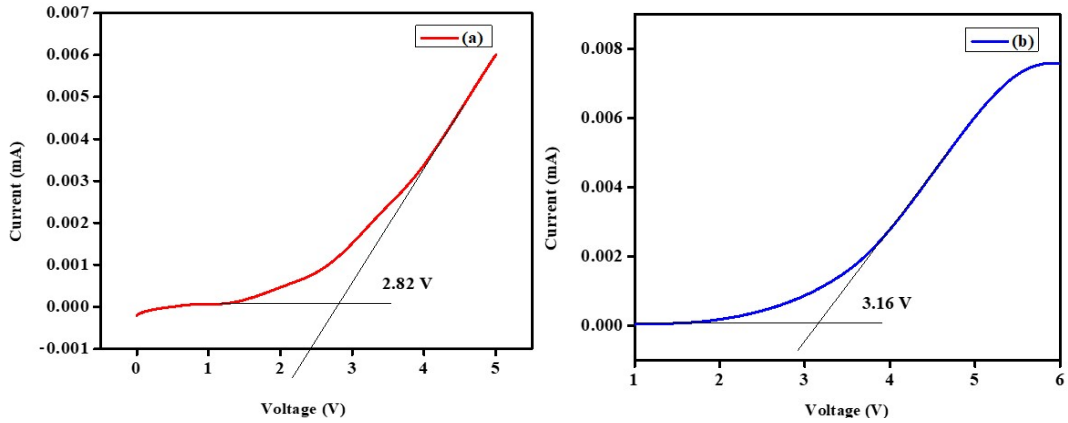

Fig. 9. Plot of Linear Sweep Voltammetry curve for the polymer membrane (a) AASCL3 and (b) AASCL3 EC1.

3.9. Cyclic voltammetry analysis (CV)

The cycling stability of the prepared electrolyte was investigated using CV analysis. In this work, the performance of the cycling stability for the highest conducting electrolyte membrane AASCL3 EC1 has been analyzed using the two-electrode setup with a scan rate of 0.1 Vs^{-1}. In this, the potential range is fixed between -3 to +3 V. The reciprocated CV pattern for the highest conducting membrane AASCL3 EC1 is depicted in Fig. 10. The result was obtained with cycling stability of 50 cycles with slight variation in its sweep area that shows the electrolyte's reversibility.

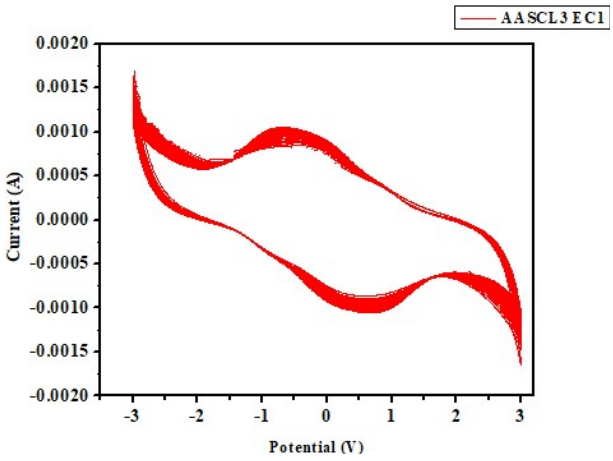

Fig. 10. Cyclic voltammetry pattern of the polymer electrolyte membrane AASCL3 EC1.

3.10. Fabrication of Battery

A primary sodium-ion battery has been fabricated using the highest ionic conducting BPE membrane AASCL3 EC1. AASCL3 EC1 as an electrolyte, sodium (Na) metal as an anode material, and V_2O_5 and MnO_2 are the two different cathode materials that were prepared and formed as the cathode pellet. The BPE membrane was placed in the battery holder between the anode and cathode. Their arrangements are shown in Fig 11. The anodic and cathodic reaction is given by

Anodic Reaction:

$$Na \rightarrow Na^{+} + e^{-}$$

Cathodic Reaction: [64,65]

$$2MnO_2 + H_2O + 2e^- \rightarrow Mn_2O_3 + 2OH^-$$

$$V_2O_5 + H_2O + 2e^- \rightarrow 2VO_2 + 2OH^-$$

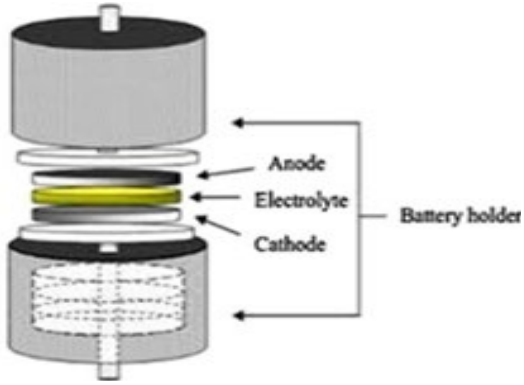

Fig. 11. Battery configuration

The open circuit voltage is monitored and displays the photographic picture for two different cathode materials (V_2O_5 and MnO_2) with AASCL3 EC1 membrane and anode (Na metal) in Fig 12 (a) and (b). The current was measured. The material of the anode, polymer electrolyte, cathode, and their open-circuit voltage and current measured are shown in Table 7.

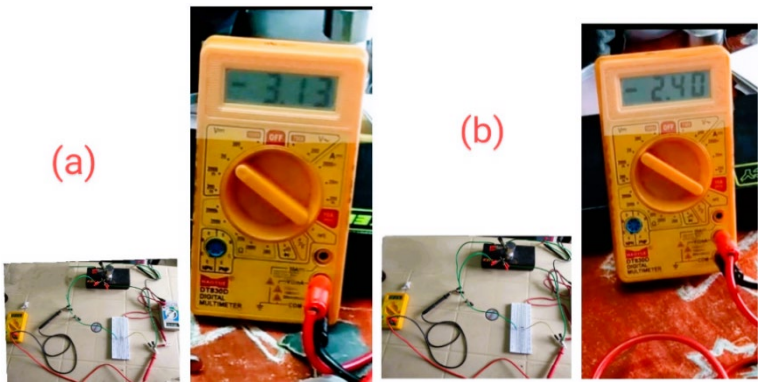

Fig. 12. Photographic picture of open circuit voltage: (a) V_2O_5, AASCL3 EC1, and sodium metal (b) MnO_2, AASCL3 EC1, and sodium metal.

Table 7. Material of anode, electrolyte, cathode, open circuit voltage, and current.

Anode	Electrolyte	Cathode	Open Circuit Voltage (V)	Current (μA)
Sodium metal	Polymer electrolyte membrane AASCL3 EC1	V_2O_5	3.13	27
Sodium metal	Polymer electrolyte membrane AASCL3 EC1	MnO_2	2.40	30

Fig.13 (a) and (b) show the open circuit voltage and discharge characteristics of the cell using anode (Na metal), electrolyte membrane AASCL3 EC1 and the cathode material V_2O_5. The OCV measurement value of the cell is 3.13 V, and it is endured for 13 h. The discharge characteristics of the constructed batteries are analyzed with a load of 100K; the voltage drops to 2.66 and remains stable.

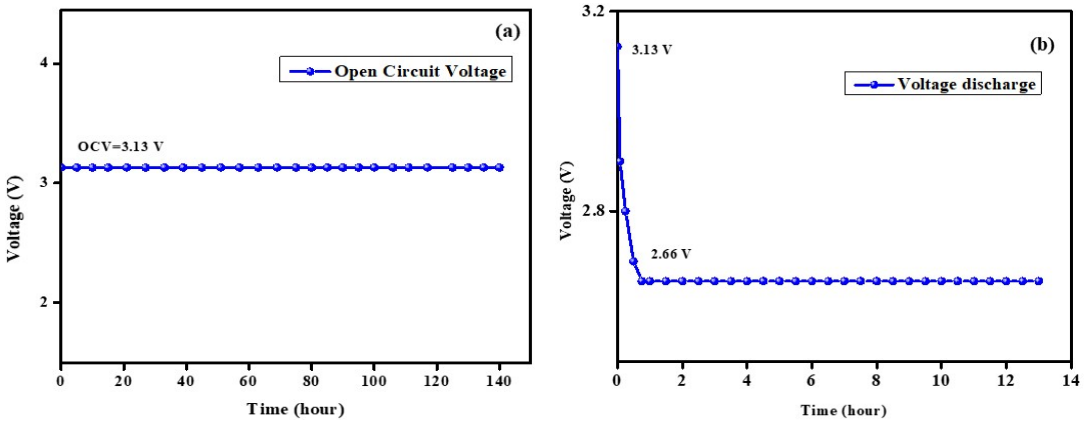

Fig. 13. (a) Plot of OCV vs. Time for the primary battery using V_2O_5, AASCL3 EC1, and anode (Na metal) (b) Plot of discharge curve for the primary battery using V_2O_5, AASCL3 EC1, and anode (Na metal)

Fig. 14 (a) and (b) show the open circuit voltage and discharge characteristics of the cell using anode (Na metal), electrolyte membrane AASCL3 EC1 and the cathode material MnO_2. The OCV measurement value of the cell is 2.40 V, and it remains stable for 13 h. The discharge characteristics of the constructed batteries are analyzed with a load of 100K; the voltage drops to 1.98 and remains stable.

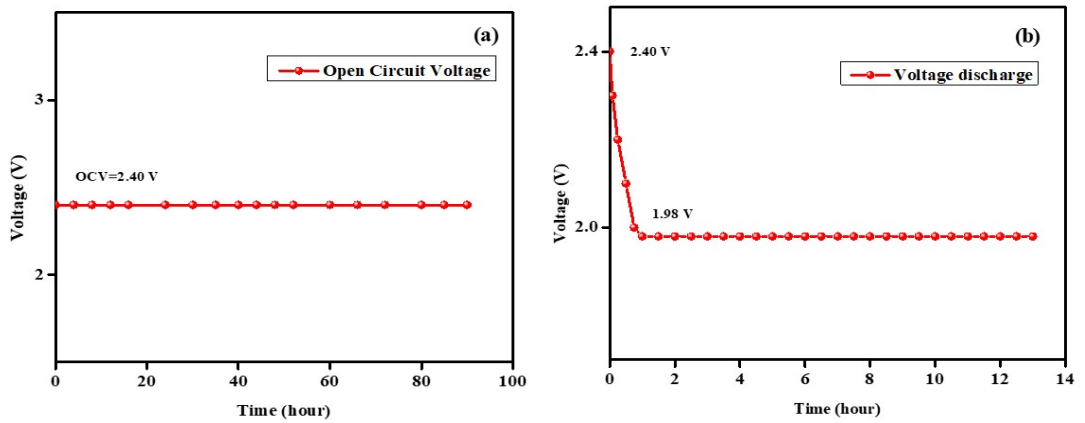

Fig. 14. (a) Plot of OCV vs. Time for the primary battery using MnO_2, AASCL3 EC1, and anode (Na metal) (b) Plot of discharge curve for the primary battery using MnO_2, AASCL3 EC1, and anode (Na metal).

Thus comparing the performance of the battery for two different cathode materials (V_2O_5 and MnO_2), the graph shows a better performance for V_2O_5 than MnO_2. This is due to the layered nature of V_2O_5.

4. Conclusion

The agar-agar: $NaClO_4$: EC-based solid biopolymer membranes were successfully prepared via a simple solution-casting technique. Enhancement of the amorphous nature of the membranes upon incorporating the $NaClO_4$ and EC has been confirmed by XRD patterns. FTIR revealed the complexation of $NaClO_4$ and EC with the host polymer. The highest ionic conductivity of 3.15×10^{-3} Scm^{-1} was achieved for the composition of 40% agar: 60% $NaClO_4$ with 0.5 wt.% of EC. DSC analysis validates the previous finding further with an extremely low T_g value of 22.05 °C for the same sample.

The promising mechanical stability of the membranes investigated via TGA verifies the membrane's usability for device construction. Transference number measurements confirm ionic conduction in prepared membranes. For the best-performing membrane, an electrochemical stability window of 3.16 V is obtained, and the cycling stability is evaluated through CV analysis. A sodium ion conducting primary battery has been assembled. The performance of a sodium ion conducting primary battery was examined using two different cathode materials, with the highest noteworthy open circuit voltage of 3.13 V achieved when V_2O_5 was employed as a cathode.

Acknowledgments

One of the authors Sowmiya Senthilnathan would like to thank the Principal and Management, Sona College of Technology for the support towards this research work. A Special thanks to Dr. C. Shanthi and Dr. S. Selvasekarapandian for their guidance.

References

[1] H. Shaghaleh, X. Xu, S. Wang, RSC Advances **8**, 825–842 (2018); https://doi.org/10.1039/c7ra11157f
[2] M. Ul Islam, S. Khan, M. W. Ullah, J. K. Park, Handbook of Composites from Renewable Materials Wiley **6**, 673–690 (2017); https://doi.org/10.1002/9781119441632.ch125
[3] K. Naveen Kumar, S. Uthanna, S. Buddhudu, IJP **5**, 159-172 (2012).
[4] P. B. Bhargav, V. M. Mohan, A. K. Sharma, V. V. R. N. Rao, Ionics **13**, 173–178 (2007); https://doi.org/10.1007/s11581-007-0102-2
[5] T. Janaki Rami Reddy, V. B. S. Achari, A. K. Sharma, V. V. R. Narasimha Rao, C. V. Subba Reddy, Journal of Physics and Chemistry of Solids. Elsevier Ltd. **69**, 1033–1036 (2008); https://doi.org/10.1016/j.jpcs.2007.10.016.
[6] E. Sheha, M. K. El-Mansy, Journal of Power Sources **185**, 1509–1513 (2008); https://doi.org/10.1016/j.jpowsour.2008.09.046.
[7] S. Rajendran, M. Sivakumar, R. Subadevi, Solid State Ionics **167**, 335–339 (2004); https://doi.org/10.1016/j.ssi.2004.01.020
[8] G. Giamonna, C. Fiorica, D. M. Stefano, F. S. Palumbo, G. Pitarresi, Journal of Pharmaceutics and Drug Development, 1 –2 (2013); https://doi.org/10.15744/2348-9782.1.e101
[9] A. M. Navarro-Suárez, J. Carretero-González, N. Casado, D. Mecerreyes, T. Rojo, E. Castillo-Martínez, Sustainable Energy and Fuels (4), 836–842 (2018); https://doi.org/10.1039/c7se00551b
[10] S. Rajendran, M. Sivakumar, R. Subadevi, Mater. Lett. **58**, 641–649 (2004); https://doi:10.1016/S0167-577X(03)00585-8
[11] S. S. Zhang, Journal of Power Sources Elsevier **162**, 1379–1394 (2006); https://doi.org/10.1016/j.jpowsour.2006.07.074
[12] P. Knauth, Solid State Ionics **180**, 911–916 (2009). https://doi.org/10.1016/j.ssi.2009.03.022
[13] T. Li, P. B. Balbuena, J. Electrochem. Soc. **146**, 3613–3622 (1999); https://doi.org/10.1149/1.1392523
[14] L. R. A. K. Bandara, M. A. K. L. Dissanayake, B. E. Mellander, Electrochimica Acta. **43**, 1447-1451 (1998). https://doi.org/10.1016/S0013-4686(97)10082-2

[15] S. Selvalakshmi, T. Mathavan, S. Selvasekarapandian, M. Premalatha, Ionics **24**, 2209–2217 (2018); https://doi.org/10.1007/s11581-017-2417-y
[16] J. S. Doa, C. P. Chang, J. Leeb, Solid State Ionics **89** (1996).
[17] H. M. J. C. Pitawala, M. A. K. L. Dissanayake, V. A. Seneviratne, Solid State Ionics **178**, 885–888 (2007); https://doi.org/10.1016/j.ssi.2007.04.008
[18] T. Matsuhashi, Elsevier Science Publishers,1–51 (1990); https://doi.org/10.1007/978-94-009-0755-3_1
[19] M. Rinaudo, Polymer International **57**, 397–430 (2008); https://doi.org/10.1002/pi.2378
[20] P. Guerrero, A. Etxabide, I. Leceta, M. Peñalba, K. de La Caba, Carbohydrate Polymers **99**, 491–498 (2014); https://doi.org/10.1016/j.carbpol.2013.08.049
[21] T. J. Madera-Santana, D. Robledo, J. A. Azamar, C. R. Ríos-Soberanis, Y. Freile-Pelegrín, Polymer Engineering and Science **50**, 585–591 (2010); https://doi.org/10.1002/pen.21574
[22] M. Atef, M. Rezaei, R. Behrooz, International Journal of Biological Macromolecules **70**, 537–544 (2014); https://doi.org/10.1016/j.ijbiomac.2014.07.013
[23] J. W. Rhim, Carbohydrate Polymers **86** (2):691–699 (2011); https://doi.org/10.1016/j.carbpol.2011.05.010
[24] T. D. Phan, F. Debeaufort, D. Luu, A. Voilley, Journal of Agricultural and Food Chemistry **53**, 973–981 (2005); https://doi.org/10.1021/jf040309s
[25] J. P. Reddy, J. W. Rhim, Carbohydrate Polymers **110**, 480–488 (2014); https://doi.org/10.1016/j.carbpol.2014.04.056
[26] J. W. Rhim, Journal of Food Science **77**, (2012); https://doi.org/10.1111/j.1750-3841.2012.02988.x
[27] B. Giménez, A. López de Lacey, E. Pérez-Santín, M.E. López-Caballero, P. Montero, Food Hydrocolloids **30**, 264–271 (2013); https://doi.org/10.1016/j.foodhyd.2012.05.014
[28] S. A. Hazaana, A. Joseph, S. Selvasekarapandian, R. M. Naachiyar, N. M. Vignesh, Journal of Solid-State Electrochemistry **27,** 539-557 (2023); https://doi.org/10.1007/s10008-022-05348-y
[29] T. J. Madera-Santana, Y. Freile-Pelegrín, J. A. Azamar-Barrios, International Journal of Biological Macromolecules **69**, 176–184 (2014); https://doi.org/10.1016/j.ijbiomac.2014.05.044
[30] Y. H. Pandya, M. Bakshi, A. Sharma, H. Pandya, Pharma Innov. J. **11**, 1151-1157 (2022).
[31] S. Y. Liew, J. C. Juan, C. W. Lai, G. T. Pan, T. C. K. Yang, T. K. Lee, Ionics **25**, 1291–1301 (2019); https://doi.org/10.1007/s11581-018-2710-4
[32] G. Hernández-Flores, A. Andrio, V. Compañ, O. Solorza-Feria, H.M. Poggi-Varaldo, Journal of Power Sources **435**, (2019); https://doi.org/10.1016/j.jpowsour.2019.226772
[33] Z. Zheng, W. Shi, X. Zhou, X. Zhang, W. Guo, X. Shi, Y. Xiong, Y. Zhu. IScience **26**, 106437 (2023); https://doi.org/10.1016/j.isci.2023.106437
[34] J. J. Kim, K. Yoon, I. Park, K. Kang, John Wiley and Sons Inc.**1** (2017); https://doi.org/10.1002/SMTD.201700219
[35] J. Yang, H. Zhang, Q. Zhou, H. Qu, T. Dong, M. Zhang, B. Tang, J. Zhang, G. Cui, ACS Applied Materials and Interfaces **11**, 17109–17127 (2019); https://doi.org/10.1021/acsami.9b01239
[36] I. Landa-Medrano, C. Li, N. Ortiz-Vitoriano, I. Ruiz De Larramendi, J. Carrasco, T. Rojo, Journal of Physical Chemistry Letters American Chemical Society **7**, 1161–1166 (2016); https://doi.org/10.1021/acs.jpclett.5b02845
[37] Q. Zhao, A. K. Whittaker, X. S. Zhao, Materials MDPI AG.**11**, (2018); https://doi.org/10.3390/ma11122567
[38] V. M. Mohan, V. Raja, A. K. Sharma, V. V. R. Narasimha Rao, Ionics **12**, 219–226 (2006); https://doi.org/10.1007/s11581-006-0035-1
[39] H. K. Koduru, M. T. Iliev, K. K. Kondamareddy, D. Karashanova, T. Vlakhov, X. Z. Zhao, N. Scaramuzza, Journal of Physics: Conference Series, **764**, (2016). https://doi.org/10.1088/1742-6596/764/1/012006
[40] K. Maithili, P. Sathya, S. Selvasekarapandian, R. Chitra, M. V. Krishna, S. Meyvel, Ionics **28**, 1783–1790 (2022); https://doi.org/10.1007/s11581-022-04440-7
[41] S. Selvalakshmi, N. Vijaya, S. Selvasekarapandian, M. Premalatha, J Applied Polymer **134**, (2017). https://doi.org/10.1002/app.44702

[42] K. Rama Mohan, V. B. S. Achari, V. V. R. N. Rao, A. K. Sharma, Polymer Testing **30**, 881–886 (2011); https://doi.org/10.1016/j.polymertesting.2011.08.010
[43] R. M. Hodge, G. H. Edward, G. P. Simon, Polymer **37**, 1371-1376 (1996); https://doi.org/10.1016/0032-3861(96)81134-7
[44] S. Rajendran, T. Mahalingam, R. Kannan, Solid State Ionics **130**, 143-148 (2000); https://doi.org/10.1016/S0167-2738(00)00283-6
[45] F. N. Jumaah, N. N. Mobaraka, A. Ahmad, N. Ramli, AIP Conference Proceedings **1571**, 768-774 (2013); https://doi.org/10.1063/1.4858748
[46] P. Buvaneshwari, T. Mathavan, S. Selvasekarapandian, M. Vengadesh Krishna, R. M. Naachiyar, Ionics **28**, 3843-3854 (2022); https://doi.org/10.1007/s11581-022-04597-1
[47] X. Zhang, X. Wang, S. Liu, Z. Tao, J. Chen, Nano Research **11**, 6244–6251 (2018); https://doi.org/10.1007/s12274-018-2144-3
[48] S. Ramesh, A. K. Arof, J Power Sources **99**, 41-47 (2001); https://doi.org/10.1016/S0378-7753(00)00690-X
[49] S. Karthikeyan, S. Sikkanthar, S. Selvasekarapandian, D. Arunkumar, H. Nithya, J. Kawamura, J Polym Res. **23**, 51–60 (2016). https://doi.org/10.1007/s10965-016-0952-2
[50] S. N. Banitaba, D. Semnani, E. Heydari-Soureshjani, B. Rezaei, A. A. Ensaf, Solid State Ionics **347**, (2020). https://doi.org/10.1016/j.ssi.2020.115252
[51] M. Forsyth, P. Meakina, D. R. MacFarlanea, J Mater Chem **7**, 193–201 (1997). https://doi.org/10.1039/A604781E
[52] K. Sundaramahalingam, M. Muthuvinayagam, N. Nallamuthu, Polym Sci Series A **61**, 565-576 (2019). https://doi.org/10.1134/S0965545X1905017
[53] S. Ramesh, R. Shanti, E. Morris, Cellulose (20) :1377-1389 (2013) https://doi.org/10.1007/s10570-013-9919-1
[54] B. A. Boukamp, Solid state Ionics **20**, 31- 44 (1986). https://doi.org/10.1016/0167-2738(86)90031-7
[55] D. R. MacFarlane, J. Sun, P. Meakin, P. Fasoulopoulos, J. Hey, M. Forsyth, Electrochim Acta. **40**, 2131–2136 (1995). https://doi.org/10.1016/0013-4686(95)00152-5
[56] C. M. Mathew, K. Kesavan, S. Rajendran, Int J Electrochem 2015. Article ID 494308 (2014). https://doi.org/10.1155/2015/494308
[57] Q. Q. Ouyang, Z. Hu, S. D. Li, W. Y. Quan, L. L. Wen, Z. M. Yang, P. W. Li, Food Chem. **264**, 277–283 (2018). https://doi.org/10.1016/j.foodchem.2018.04.098
[58] R. D. Alves, L. C. Rodrigues, J. R. Andrade, A. Pawlicka, L. Pereira, R. Martins, E. Fortunato, M. M. Silva, Mol. Cryst. Liq. Cryst. **570**, 1–11 (2013).https://doi.org/10.1080/15421406.2012.703041
[59] A. F. Fuzlin, A. S. Samsudin, J. Polym.Bull. **78**, 2155-2175 (2021).https://doi.org/10.1007/s00289-020-03207-2
[60] N. A. Nik Aziz, N. K. Idris, M. I. N. Isa, J. Phys Sci **5**:748-752 (2010).
[61] J. B. Wagner, C. Wagner, J. Chem. Phys. **26**, 1597-1601 (1957). https://doi.org/10.1063/1.1743590
[62] M. A. Ramlli, M. I. N. Isa, J. Phys. Chem B **120**, 11567-11573 (2016). https://doi.org/10.1021/acs.jpcb.6b06068
[63] R. N. Elizabeth, S. Kalyanasundaram, Y. Saito, A. M. Stephan, Polimeros **15**, 46–52 (2005). https://doi.org/10.1590/S0104-14282005000100011
[64] T. Ponraj, A. Ramalingam, S. Selvasekarapandian, S. R. Srikumar, R. Manjuladevi, Polymer Bulletin (78), 35-57 (2020). http://doi.org/10.1007/s00289-019-03091-5
[65] R. Tamilisai, P. N. Palanisamy, S. Selvasekarapandian, T. Maheshwari, J Mater Sci: Mater Electron (32), 22270-22285 (2021). http://doi.org/10.1007/s10854-021-06713-9